A novel method of embedding distributed optical fiber sensors for structural health monitoring

2011 Smart Mater. Struct. 20 125018

(http://iopscience.iop.org/0964-1726/20/12/125018)

Smart Mater. Struct. **20** (2011) 125018 (9pp) doi:10.1088/0964-1726/20/12/125018

A novel method of embedding distributed optical fiber sensors for structural health monitoring

J H Mao[1], W L Jin[1,2], Y He[1], D J Cleland[3] and Y Bai[3]

[1] Institute of Structural Engineering, Zhejiang University, Hangzhou, 310058, People's Republic of China
[2] Ningbo Institute of Technology, Zhejiang University, Ningbo 315100, People's Republic of China
[3] School of Planning, Architecture and Civil Engineering, Queen's University of Belfast, BT9 5AG, Belfast, UK

E-mail: heyong_ise@zju.edu.cn

Received 14 June 2011, in final form 1 October 2011
Published 28 November 2011
Online at stacks.iop.org/SMS/20/125018

Abstract
A distributed optical fiber sensor based on Brillouin scattering (BOTDR or BOTDA) can measure and monitor strain and temperature generated along optical fiber. Because it can measure in real-time with high precision and stability, it is quite suitable for health monitoring of large-scale civil infrastructures. However, the main challenge of applying it to structural health monitoring is to ensure it is robust and can be repaired by adopting a suitable embedding method. In this paper, a novel method based on air-blowing and vacuum grouting techniques for embedding long-distance optical fiber sensors was developed. This method had no interference with normal concrete construction during its installation, and it could easily replace the long-distance embedded optical fiber sensor (LEOFS). Two stages of static loading tests were applied to investigate the performance of the LEOFS. The precision and the repeatability of the LEOFS were studied through an overloading test. The durability and the stability of the LEOFS were confirmed by a corrosion test. The strains of the LEOFS were used to evaluate the reinforcing effect of carbon fiber reinforced polymer and thereby the health state of the beams.

(Some figures may appear in colour only in the online journal)

1. Introduction

Due to the change of external environment and the deterioration of material, decline of structural health status becomes an important issue. Structural health monitoring (SHM) refers to the use of *in situ*, nondestructive sensing and analysis of system characteristics, including structural response, for the purpose of detecting changes, which may be used to indicate damage or degradation [1]. In general, a typical SHM system includes three major components: sensor system, data processing system and health evaluation system. Many kinds of sensors have been used to integrate the sensor system [2]. Benefiting from its advantages in small size, high precision, good durability and insensitivity to electrical magnetic interference, fiber optical sensors promise to be an alternative sensing technique in SHM systems and future smart structures [3].

The distributed optical fiber sensor based on Brillouin scattering (BOTDA or BOTDR) not only possesses the common advantages of optical fiber sensors, but also has the characteristic of distributed monitoring. It is quite convenient for large-scale SHM, such as dam, tunnel, bridge, slope etc. However, the optical fiber sensors involved in those projects were bonded on the surface of structures [4–7]. It is not a safe and stable way to ensure optical fiber sensors run for the whole life of civil engineering infrastructure, because the sensors on the surface may be damaged by chemical attack, mechanical impact, material deterioration or even man-made interference. In addition, if the sensors could be embedded into concrete, not only life-cycle structural health monitoring could be carried out, but also interior strain could be recorded. However, because of its fragility, it is impossible to embed optical fiber sensor into concrete directly without any packaging. Sensors packaged by fiber reinforced polymer or composite materials have been invented and applied to practical projects [8]. Although the special packaged sensors have sufficient strength to survive from concrete casting, the segmental embedding method has to be adopted in order to avoid higher damage risk as monitoring range increases. In that case, many fiber splicings are needed to link the whole monitoring net, which would increase the light loss and, hence, reduce the measuring range. On the other hand, there is a limitation on the life of an optical fiber, so a replacement or an update needs to be considered. Otherwise, it is difficult to achieve life-cycle SHM.

In this paper, a novel embedding method for long-distance optical fiber sensors is developed based on the air-blowing and vacuum grouting technique. The long-distance embedded optical fiber sensor (LEOFS) is installed into concrete by three main steps: embedding tubes (both main tubes and spare tubes) with small diameter at the desired position; applying an air-blowing technique to lay optical fiber into the pre-installed tubes; utilizing the vacuum grouting technique to fix optical fiber tightly inside the tubes. An experiment to simulate this embedding method was carried out. The results showed that the maximum laying length could reach to 500 m. Therefore once all tubes had been embedded into concrete during construction, the installation and even the replacement of LEOFS could be easily operated. In order to learn the performance of the LEOFS, two stages of static loading tests were applied to reinforced concrete beams containing embedded LEOFS. During the first static loading test, the precision and the repeatability of the LEOFS were studied. Then the durability and the stability of the LEOFS were investigated by corrosion tests. The second static loading test was imposed on the repaired beams which had been strengthened by carbon fiber reinforced polymer (CFRP). By comparing the strains measured by the LEOFS in these two-stage static loading tests, the condition of the beams and also the reinforcing effect of CFRP were evaluated.

2. Background theory

2.1. Distributed optical fiber sensing technology

The interaction between incident light waves and acoustic phonons in optical fiber generates Brillouin scattered light as backscattered light, it propagates along the direction opposite to the incident light waves. When there are strain or temperature variations, the Brillouin frequency will shift. The frequency shift has a linear relationship with strain and temperature, it is expressed as [9].

$$\Delta \upsilon_{\mathrm{B}}(\varepsilon, T) = \frac{\mathrm{d}\upsilon_{\mathrm{B}}(T)}{\mathrm{d}T}\Delta T + \frac{\mathrm{d}\upsilon_{\mathrm{B}}(\varepsilon)}{\mathrm{d}\varepsilon}\Delta\varepsilon. \tag{1}$$

There is no coupling relationship between temperature change (ΔT) and strain variation ($\Delta\varepsilon$) when the Brillouin frequency shift ($\Delta\upsilon_{\mathrm{B}}(\varepsilon, T)$). Free optical fiber sensor without any bonding to structure could be used as a temperature compensation sensor by laying it beside a strain monitoring sensor.

The distance (Z) of strain varying or temperature changing can be determined from the following equation.

$$Z = \frac{ct}{2n}. \tag{2}$$

In equation (2), c is the light velocity in vacuum, n is the refractive index of an optical fiber, and t is measuring time.

2.2. Air-blowing technique

The fabrication of the LEOFS is based on air-blowing and vacuum grouting, the LEOFS had been applied to a tunnel health monitoring by the authors [10, 11]. The air-blowing technique for the installation of optical fiber was introduced in the 1980s [12]. Compared to conventional optical fiber cable laying techniques, its installation time can be minimized, furthermore it enables a 'dynamic' network where fibers can be added, removed or replaced. Now it is widely used in the field of optical fiber communication by using compressed air. The pressure difference between two ends of the tubes forms the driving force to draw fiber from one end to the other. Researchers had proved that there was no harmful influence on the optical fiber. As a kind of mature technique, software used for estimating the installation length has been developed [13].

2.3. Vacuum grouting technique

Grouting is an important step in post-tensioned concrete construction, which is used for protecting pre-stressing tendons from corrosion [14]. The vacuum grouting technique not only enhances grout's compactness, but also increases the grouting length. In order to ensure that fiber sensors inside the tubes can sense structural strain, the internal space between fiber and tube must be filled tightly. The vacuum grouting technique can achieve this purpose to form the LEOFS.

3. Fabrication of the LEOFS

The monitoring sensor nets are firstly designed to meet the objectives of SHM. Then tubes are fixed to formwork or steel bars before concrete casting. Finally air-blowing and vacuum grouting techniques are used for laying the distributed optical fibers and fixing them inside the tubes to form the LEOFS.

However, special techniques are required when applying the air-blowing technique to install distributed optical fiber sensors in civil engineering. Due to the fact that segmental concrete casting is always needed to avoid large volume concrete construction, more connectors are needed to link all tubes in concrete together to form an air-blowing network. Therefore, unlike optical fiber communication, the resistance-like loss of air pressure and unevenness between tubes caused by the connectors will increase the difficulty of air-blowing. Therefore it is necessary to carry out a simulation experiment to estimate the maximum length for the LEOFS's installation. The experimental layout is shown in figure 1. The flowing velocity of optical fiber into tube was measured by a speed recorder.

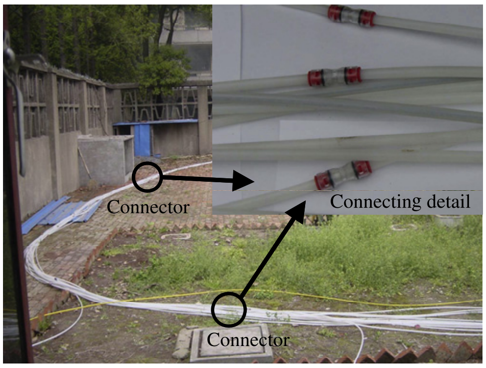

Figure 1. Layout of the simulation experiment, the tubes with 16 mm diameter were linked by connectors every 12 m.

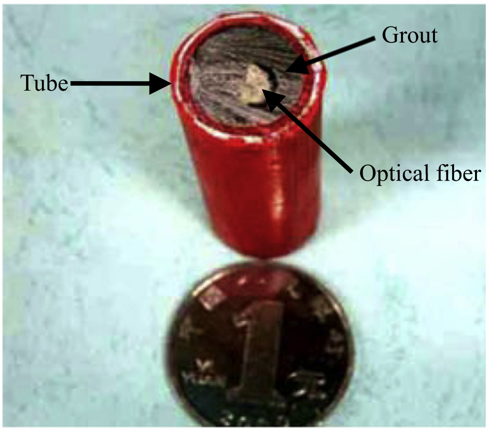

Figure 2. Configuration of the LEOFS.

The results show that the velocity remained at a high level above 50 m min^{-1} before 300 m, and then the speed decreased as length increased. Although the velocity had decreased to 20 m min^{-1} in the end, the one-time maximum length could reach 500 m.

While applying the vacuum grouting technique to fabricate the LEOFS, two additional technical obstacles have to be overcome: long length and small diameter of tube. Therefore, it is necessary to develop a new grouting mixture which can provide a high fluidity, a reasonable expansion rate and a longer setting time. The authors have invented an optimal proportion among cement, water, air entraining agent, water-reducer, expansive agent and cement retarder and applied a Chinese patent (CN1765812). By using this new grout mixture, 500 m can be achieved while grouting inside tubes with 16 mm diameter. Figure 2 illustrates the structure of the LEOFS.

In order to make the laying length of the LEOFS longer than 500 m, the optical fiber exiting at the end of one segmental tube (one 500 m) can be laid into the following segmental tube (another 500 m). Therefore the total length of the LEOFS's installation can reach several kilometers without any splicing.

The tubes adopted in figure 2 and the following experiments are made of aluminum and plastic with 16 mm diameter. The plastic layer prevents harmful iron invading; meanwhile the aluminum layer between two plastic layers provides enough rigidity to ensure it survive the concrete casting. In order to ensure the SHM sensor system works during the whole structural life, a replacement and an update of the optical sensor should be considered. A set of spare tubes for new fiber sensors installed at a later date can extend the life of an SHM sensor system.

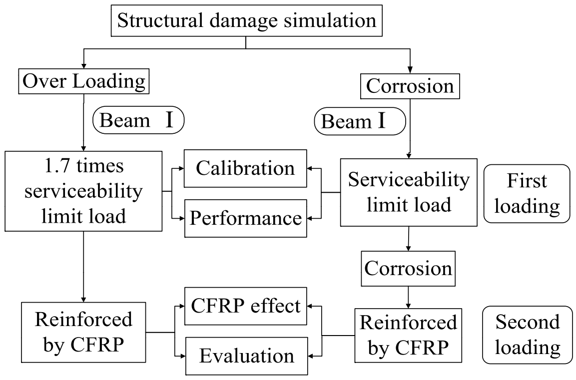

Figure 3. Flow chart of experiments.

4. Experiment design

The most common causes leading to structural damage in RC structures are overloading and reinforcement corrosion. The LEOFS can monitor and record the structural condition immediately after the completion of construction, and this data could form a database for evaluating structural health status in the future. In order to verify its validity for SHM, experiments were designed, as shown in figure 3.

The cross-section of the beam is 150 mm × 300 mm and its length is 2600 mm. The concrete grade is designed as C30, and two HRB 335 steel bars with 16 mm diameter acted as the main reinforcement. To simulate overloading, a load equal to 1.7 times the serviceability limit load was applied to beam I. Then beam I was strengthened by adhering CFRP sheets on its bottom. A load equal to the serviceability limit load was applied to beam II, and then the accelerated corrosion test was carried out to simulate reinforcement corrosion. After the corrosion test, beam II was strengthened in the same way as beam I.

The calibration and performance investigation of the LEOFS were deduced from the first static loading test, and meanwhile the initial condition of each beam was recorded. During the second static loading test, the strengthening effect of CFRP was assessed by comparing the strain measured from two steps of the static loading tests. Static loading tests were utilized to simulate the overloading condition for beam I and the load carried by the beam before corrosion initiated for beam II. In order to evaluate the beam's health status effectively, the same arrangements of loading and data collection were applied. The details of all sensors are shown in figure 4.

The distances of the LEOFSs from the bottom of the beam were 25, 50 and 275 mm. The LEOFSs at 25 mm (LS_{25}) and 275 mm (LS_{275}) were used for calibration purposes, which were achieved by comparing the strain from the LEOFS with that from the electrical resistance strain (ERS) gauge.

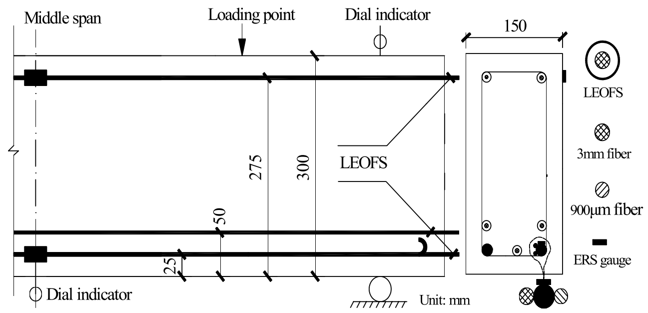

Figure 4. Details of sensor arrangement for the static loading tests.

Table 1. Sensor arrangement.

Label	Position	Object
LS_{25}	25 mm from bottom	Calibration
LS_{50}	50 mm from bottom	Repeatability analysis
LS_{275}	275 mm form bottom	Repeatability analysis
ERS_T	Surface of steel bar	Calibration for LS_{25}
ERS_C	Surface of concrete	Calibration for LS_{275}
F_3	Surface of steel bar	Calibration
$F_{0.9}$	Surface of steel bar	Calibration for F_3

The ERS gauges were bonded at two different positions: the tensile ERS gauge used for LS_{25} calibrating was bonded on the surface of the main reinforcement; the compressive ERS gauge used for LS_{275} calibrating was bonded on the surface of the concrete. The repeatability of tensile strain measurement was assessed by comparing the two LEOFSs (LS_{50}) at a height of 50 mm, and compressive strain by the two LEOFSs (LS_{275}) at a height of 275 mm. Because the fiber used for the LEOFSs fabrication must meet the requirements of strength and rigidity for the air-blowing technique, optical fiber for the LEOFSs was specially manufactured by adding a jacket with 3 mm diameter as protection. Because of the low elastic modulus of the jacket, the increase of the jacket's thickness would reduce its sensitivity to strain sensing [3, 15], the performance of the optical fiber covered with the 3 mm jacket needs to be learned by comparing with 900 μm fiber which is commonly used as a strain monitoring fiber. All sensors are listed in table 1.

4.1. Static loading test

A four-point load was applied in the static loading test so that a segment with 1.0 m uniform bending moment could be formed. For each loading step, the load was held constantly for 10 min before acquiring data. The fiber strains were monitored three times automatically by BOTDA (DITEST STA-R BOTDA, product of Omnisens SA Co.) at each load level, and the average values were used for the final analysis. A supplementary fiber which was not subjected to strain was set beside the beam so that the measured strain could be used to eliminate the temperature effect. The minimal spatial resolution of BOTDA is 0.5 m and its measuring accuracy is $20\mu\varepsilon$. In order to obtain more sample points from the uniform bending section, 0.5 m spatial resolution and 0.1 m sampling distance were set up. The deformation of the beam was recorded by a dial indicator. The layout of the experiment is shown in figure 5.

Figure 5. Layout of the static loading test.

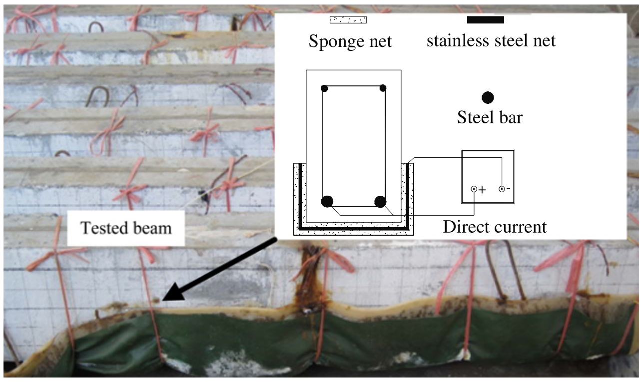

Figure 6. Layout of the corrosion test.

4.2. Corrosion test

For the purpose of corrosion simulation, an accelerated corrosion test as illustrated in figure 6 was adopted to beam II following first static loading test. The steel bars were connected to the positive pole of a direct current, while a stainless steel net was connected to the negative pole. The electrical field could accelerate the immigrating speed of chloride to the surface of steel bars, and then enhance the corrosion rate. Current density was kept consistent at 0.01 mA cm^{-2} during the whole corrosion test. Sponge wrapped around the beam section was saturated with 5% NaCl saltwater solution.

As a result of steel corrosion, the volume of the steel bars enlarged, and the concrete cover cracked along the length of the steel bars. This test lasted more than two months until remarkable corrosion cracks were observed. The average width and total length of corrosion cracks reached 0.6 mm and 1.1 m respectively by the end of the test.

4.3. Strengthening by CFRP

The damaged beams from the overloading test (beam I) and the corrosion test (beam II) were repaired using CFRP. One layer of CFRP was bonded on the bottom of the beams, and then anchored by a U shape CFRP band, as shown as figure 7.

The thickness of the CFRP is 0.111 mm; its ultimate tensile strength is bigger than 3500 MPa. In order to bond the CFRP tightly to the bottom, the loose concrete around cracks caused by overloading or corrosion testing were cleaned away

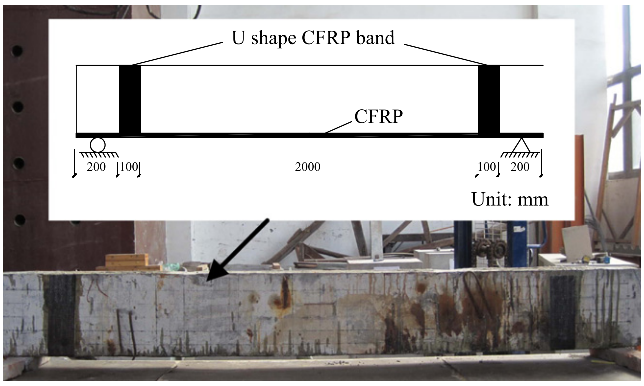

Figure 7. CFRP strengthening arrangement.

and smoothed by epoxy resin. Then the second static loading test was applied to the repaired beams; the same loading processes as the first loading test were considered.

5. Results and discussion

Strain is the most important and intelligible information to evaluate the health status of any structures. In the interest of life-cycle health monitoring, sensors need to remain working throughout the whole life of the structure. As experiments progressed, some ERS gauges were unfortunately broken or their results became distorted. However, fiber optical sensors can record the strain for the whole experimental process. The results are shown in figure 8. According to the layout of the sensors (figure 4), there were seven different sensing areas along the embedded fiber which are clearly displayed in figures 8(a) and (c). But the sensing areas were reduced during the second static loading test after strengthening by the CFRP, as shown in figures 8 (b) and (d). The reason is that the redundant fibers used for connecting each sensor were destroyed during moving and installation. Fortunately, some sensors could be used again after being repaired by splicing.

In order to carry out calibration and repeatability analysis, comparisons of strain between fiber sensors and ERS gauges are needed. The strains of ERS gauges are point-wise, which means only the strain of the beam's middle span is measured. However, distributed optical fiber sensors measure all the strain along the beam. Therefore, the sample point of the fiber sensor which is located in the middle span has to be recognized. According to the spacing of sample points (0.1 m), several sample points can represent the strain of a pure bending section. However, due to the limitation of spatial resolution and the systemic measuring error, it is not easy to locate these points manually; a method based on software (Matlab) was developed to recognize the desired sample point automatically.

5.1. Strain in pure bending section

As a distributed testing technique, the limit of minimal spatial resolution is the main disadvantage of BOTDA. The spatial resolution is determined by pulse width (τ) of incident light. The spatial resolution (ΔZ) is expressed using a given pulse width (τ) as

$$\Delta Z = \nu\tau/2 \tag{3}$$

Here ν is the light velocity in the optical fiber. The strain of each sample point is gained by averaging all strains of the spatial resolution [16, 17]. However, the designated spatial location of the sample point and also integrating kernel would affect the shape of the strain curve. This is illustrated in figure 9.

Two different spatial resolutions (0.5 and 1.0 m) had been utilized to recognize the sample point which was located in the middle of the beam. Three different designated spatial locations of sample point were assumed. Case I: the start of the interval (figure 9(b)); case II: the midway of the interval (figure 9(c)); case III: the end of the interval (figure 9(d)). Different types of BOTDA equipment have their own integrating model. In this paper, a uniform integration kernel model has been used as a simplified method. Learned from figures 9((b)–(d)), there should be no spatial bias shift for case II; the strain curve of 1.0 m spatial resolution is moved forward and back for case I and case III respectively.

Taking LS_{25} (18 kN) of beam I for example, the measured strain curve is plotted in figure 10. By comparing figure 10 with 9((b)–(d)), the shape of the strain curve is similar to figure 9 (b). So the assumption that the designated spatial location is at the start of the interval is reasonable.

According to figure 9(b), while testing with 1.0 m spatial resolution, only one sample point is located entirely in the pure bending section. Whilst for 0.5 m spatial resolution, there are five sample points existing within the pure bending section. But it is difficult to identify the five points for the test by 0.5 spatial resolutions, because the measurement error ($\pm 20\mu\varepsilon$) could make the strain curve fluctuate a little, as shown in figure 10. Taking the average value of five points as the real strain of a pure bending section, there would be several choices, such as the strain for choice A being $666\mu\varepsilon$, but for choice B it is $646\mu\varepsilon$. This difference should be eliminated by developing a practical recognition method.

Figure 11 is plotted by subtracting a strain of 0.5 m spatial resolution from 1.0 m (figure 10). According to figure 9(b), there is a sample point whose difference between 0.5 and 1.0 m is equal to zero, and the next four sample points following this sample point are also located at a pure bending section in 0.5 m spatial resolution testing. Therefore, this point can be considered as a judge point for the start point of a pure bending section by a 0.5 m spatial resolution test. Taking the case in figure 10, this judge point with the smallest absolute difference is located at 1.5 m. The judge point is the start point of section C in figure 10. This method can avoid the error caused by manual selection, because the automatic recognition program based on Matlab or other software can be easily achieved. The fiber strains in this paper were calculated by this method.

5.2. Performance of the LEOFS

Figure 12(a) compares the strains of ERS gauges and that of fiber sensors in the tensile area, and figure 12(b) for the compressive area. A good relationship between fiber sensor and ERS gauges is obviously displayed in both the tensile and compressive areas. It can be seen from figure 12(a) that the stains of steel bars detected by the fiber sensors with 3 mm

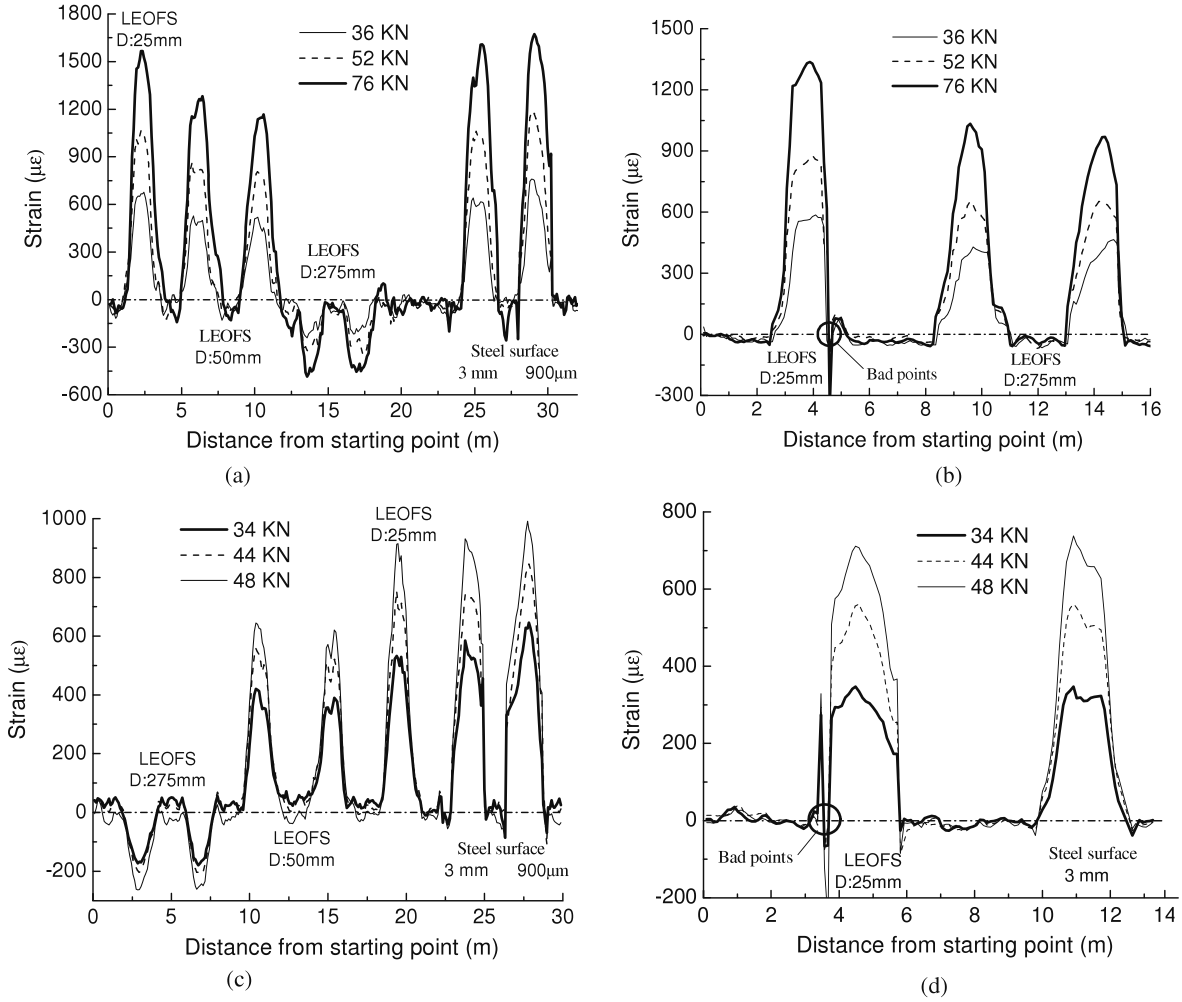

Figure 8. Strain of the beams recorded by BOTDA: (a) strain of beam I before strengthening, (b) strain of beam I after strengthening, (c) strain of beam II before strengthening and (d) strain of beam II after strengthening.

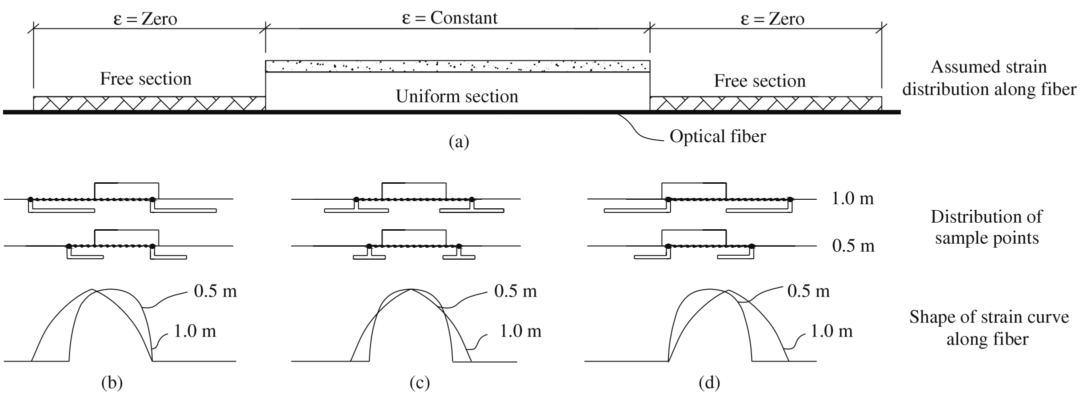

Figure 9. Influence of spatial resolution on the strain monitor: (a) assumed strain distribution along the fiber, (b) designated spatial location at the start of the interval, (c) designated spatial location at the midpoint of the interval, (d) designated spatial location at the end of the interval.

diameter (F_3) are smaller than that of the sensors with 900 μm diameter ($F_{0.9}$). Nonetheless, the 3 mm fibers have to be selected for the air-blowing, because additional strength is needed for air-blowing operation.

The LS_{25} sensor and the F_3 sensor were made up using the same sensing fiber, i.e. the fiber covered with the 3 mm jacket, and also they were embedded into beams at the same height. It can be seen that the measured strains from these two sensors are very close (figure 12(a)). The main difference between the LS_{25} sensor and the F_3 sensor is that the former also contains the grout and the tube in addition to the 3 mm fiber. These results would suggest that the embedding methods

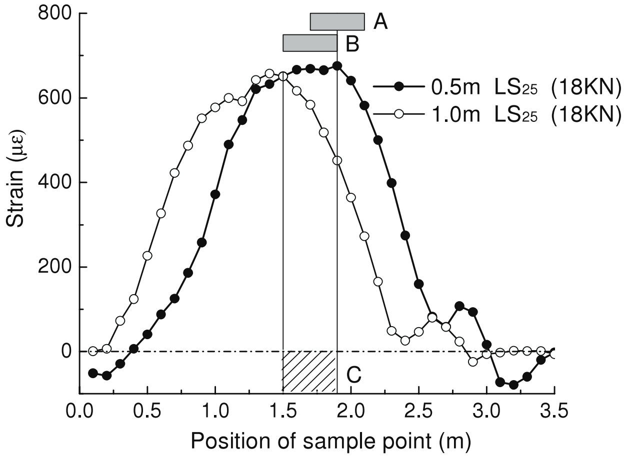

Figure 10. Experimental strain distribution.

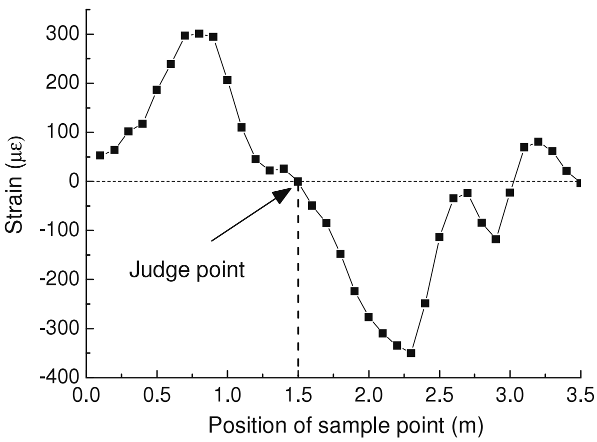

Figure 11. Judge point recognition.

of air-blowing and vacuum grouting have little influence on strain measurement. The reason is that the low elastic modulus of tube and grout reduced its sensitivity to strain sensing. The same phenomena can be seen in figure 13(b) which presents the compressive strains. It is clear that the LEOFS can effectively detect the strain both in the tensile and the compressive areas.

A sensor system for SHM needs to possess stability and repeatability. Two pairs of LEOFS sensors were embedded at the same height, one pair in the tensile and the other in the compressive areas, their detailed positions are shown in figure 4. The strains are presented in figure 13.

From figure 13, good repeatability of the LEOFS is observed both in the tensile and the compressive areas. The average difference of each sensor is $20\mu\varepsilon$, which is in an acceptable range.

5.3. *Strengthening effect evaluation*

The second static loading test was carried out to evaluate the performance of the CFRP strengthened beams. The ERS gauges bonded to the surface of the steel bars could not sense the strain after two months. Though some fiber sensors were damaged during the moving and the installation, most were sufficiently reliable to keep working during the whole experiment. The results are presented in figure 14.

It can be seen from figures 14(a) and (b) that the strain measured by the LEOFSs within the tensile zone of both beams after strengthening by the CFRP was smaller than those recorded before strengthening, respectively. It means that after strengthening by the CFRP, strains of the concretes in the tensile zone of the beams were reduced and therefore the load capacity was probably enhanced. It was discovered from the experiments that the LEOFS can be used as the sensor system for long-term SHM.

6. Conclusions

A novel method for embedding long-distance optical fiber sensors into concrete based on air-blowing and vacuum grouting was developed. This method can solve the major obstacle of installing the distributed optical fiber sensor into concrete. It was fabricated by three main steps: embedding small diameter tubes at the desired position; using the air-blowing technique to lay fiber sensor into the pre-installed

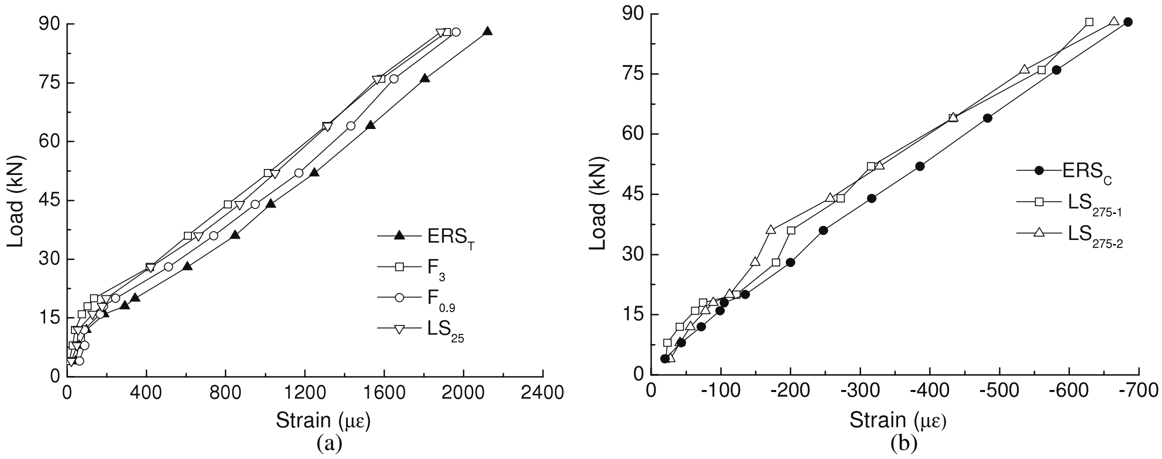

Figure 12. Performance analysis of LEOFS sensor: (a) performance of LEOFS sensor at tensile area and (b) performance of LEOFS sensor at compressive area.

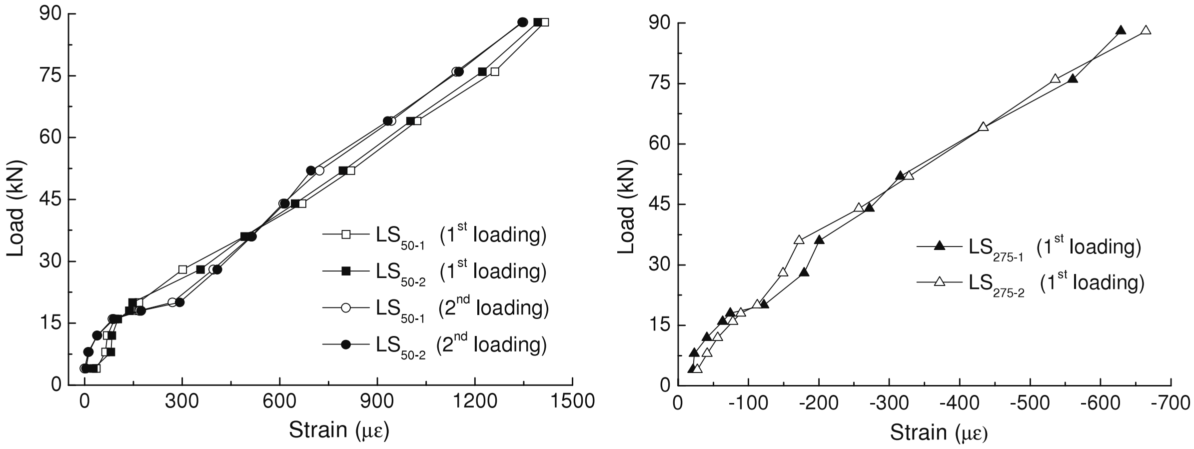

(a) (b)

Figure 13. Repeatability analysis of the LEOFS sensor: (a) performance of the LEOFS sensor for a tensile area and (b) performance of the LEOFS sensor for a compressive area.

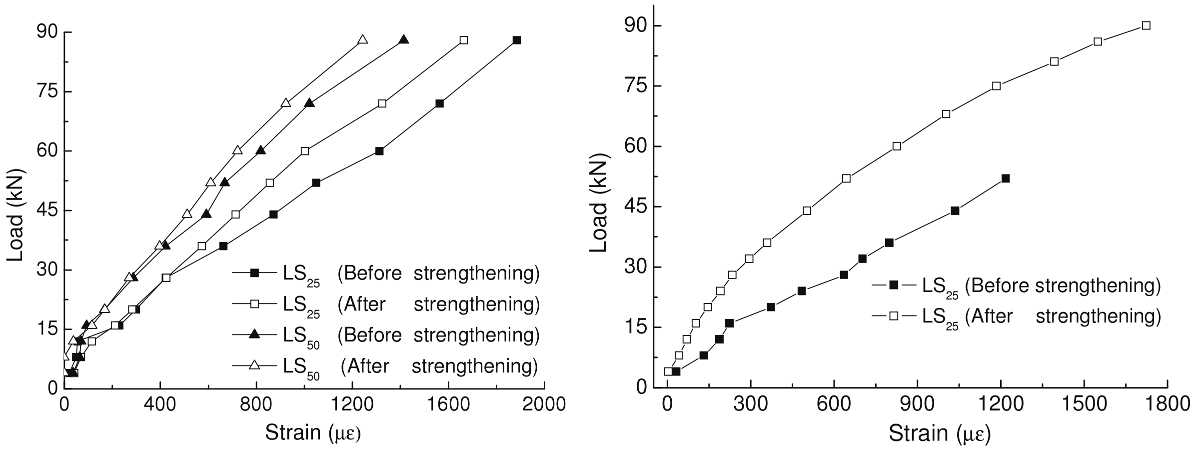

(a) (b)

Figure 14. Evaluation of CFRP strengthening effect for each beam by comparing strain of the two stages' loading tests: (a) strain comparison for beam I, (b) strain comparison for beam II.

tubes; utilizing the vacuum grouting technique to fix the fiber sensor tightly inside the tubes. Based on the current experimental results, the principal conclusions are listed as:

(1) The simulation experiment of this novel embedding method shows that the one-stage laying length could reach 500 m. Spare tubes placed inside concrete can be used for renewing the LEOFS to achieve health monitoring during the whole life of structures.
(2) Once all tubes were embedded into the concrete during construction, the installation as well as the replacement could be conveniently carried out by the professional air-blowing and vacuum grouting techniques. The whole embedding process has no interference with normal concrete construction.
(3) During a static loading test, the LEOFSs were demonstrated to have the necessary precision and repeatability. The durability and stability of the LEOFSs were proved through overloading and corrosion tests. The results show that the LEOFS is suitable for long-term structural health monitoring.
(4) In addition to the general monitoring applications, the LEOFS also could be used for evaluating the effect of structural strengthening.

Acknowledgment

The research was supported by the Zhejiang Provincial Natural Science Foundation of China (no. Y1110323), Projects of International Cooperation and Exchanges NSFC (no. 50920105806) and Project of Ministry of Science and Technology of China (no. S2011Z10100).

References

[1] Housner G W, Bergman L A, Caughey T K, Chassiakos A G, Claus R O, Masri S F, Skelton R E, Soong T T, Spencer B F and Yao J 1997 Structural control: past, present, and future *J. Eng. Mech.* **123** 897–971
[2] Chang P C, Flatau A and Liu S C 2003 Review paper: health monitoring of civil infrastructure *Struct. Health Monit.* **2** 257–67

[3] Li H N, Li D S and Song G B 2004 Recent applications of fiber optic sensors to health monitoring in civil engineering *Eng. Struct.* **26** 1647–57

[4] Shi B, Xu X J, Wang D, Wang T, Zhang D, Ding Y, Xu H Z and Cui H L 2005 Study on BOTDR-based distributed optical fiber strain measurement for tunnel health diagnosis *Chin. J. Rock Mech. Eng.* **24** 2622–8 (in Chinese)

[5] Matta F, Bastianini F, Galati N, Casadei P and Nanni A 2008 Distributed strain measurement in steel bridge with fiber optic sensors: validation through diagnostic load test *J. Perform. Construct. Facil.* **22** 264–73

[6] Broennimann R, Nellen P M, Anderegg P and Sennhauser U J 1998 Application of optical fiber sensors on the power dam of Luzzone *Proc. SPIE* **3407** 386–91

[7] Kato S and Kohashi H 2006 Study on the monitoringsystem of slope failure using optical fiber sensors *Proc. GeoCongress: Geotechnical Engineering in the Information Technology Age* vol 2006, pp 34–9

[8] Zhou Z, He J P, Yan K and Ou J P 2008 Fiber-reinforced polymer-packaged optical fiber sensors based on Brillouin optical time-domain analysis *Opt. Eng.* **47** 14401

[9] Kwon I B, Kim C Y and Choi M Y 2003 Distributed strain and temperature measurement of a beam using fiber optic BOTDA sensor *Proc. SPIE* **5057** 486–96

[10] Mao J H, Jin W L and He Y 2010 Structural health monitoring based on long-distance embedded optical fiber sensor *Proc. 2nd Int. Conf. on Durability of Concrete Structures* pp 127–35

[11] Mao J H, He Y and Jin W L 2010 Method for tunnel life-cycle health monitoring based on distributed optical fiber sensor *Proc. 7th Int. Symp. on Structural Engineering* vol 1, pp 1064–9

[12] Cassidy S, Yennadhiou P and Reeve M 1986 The blown fiber cable *IEEE J. Sel. Areas Commun.* **4** 679–85

[13] Griffioen W, Plumettaz G and Nobach H G 2006 Theory, software, testing and practice of cable in duct installation *Proc. 55th Int. Wire and Cable Symp.* pp 357–65

[14] Minh H, Mutsuyoshi H and Niitani K 2007 Influence of grouting condition on crack and load-carrying capacity ofpost-tensioned concrete beam due to chloride-induced corrosion *Construct. Build. Mater.* **21** 1568–75

[15] Ansari F and Libo Y 1998 Mechanics of bond and interface shear transfer in optical fiber sensors *J. Eng. Mech.* **124** 385–94

[16] Zhang H and Wu Z S 2008 Performance evaluation of BOTDR-based distributed fiber optic sensors for crack monitoring *Struct. Health Monit.* **7** 143–56

[17] Ding Y, Shi B and Zhang D 2010 Data processing in BOTDR distributed strain measurement based on pattern recognition *Opt.-Int. J. Light Electron Opt.* **121** 2234–9